Single-Valued DMBE Potential Energy Surface for HSO: A Distributed *n*-Body Polynomial Approach

E. Martínez-Núñez and A. J. C. Varandas*

Departamento de Química, Universidade de Coimbra, P-3049 Coimbra, Portugal

Received: January 11, 2001; In Final Form: March 27, 2001

An accurate single-valued double many-body expansion (DMBE) potential energy surface is reported for the ground electronic state of HSO based on novel MR CISD ab initio energies suitably corrected for the complete one-electron basis set/complete CI limit. To improve the accuracy of the fit, we have suggested a *n*-body distributed polynomial approach which implies using individual multinomial developments at the various stationary points. For simplicity, only the three most relevant such points have been considered: two minima (HSO, HOS) and the saddle point connecting them.

1. Introduction

The chemistry of atmospheric sulfur is of great interest due to its importance in environmental issues. In particular, a considerable number of experimental studies have been reported for the $O(^3P) + H_2S$ system.[1−6] Goumri et al.[7] studied the geometrical features and energetics for the minima and 11 transition states of this system at the MP2=FULL/6-31G(d) and Gaussian-2 (G-2) levels of theory. They have also calculated canonical transition state theory rate coefficients for the various channels arising from the $O(^3P) + H_2S$ reaction and compared with experiment. For a complete analysis of the experimental results, a classical and/or quantum dynamics study would therefore be desirable. For this purpose, one requires to construct a global potential energy surface for the H_2OS system. As a first step in this construction, potential energy surfaces surfaces must be provided for the various fragments. Among them is HSO, which is an important molecule per se in atmospheric chemistry. In particular, it may be involved in a so-called catalytic cycle[8−10] for destruction of ozone in the troposphere, namely

$$HS + O_3 \rightarrow HSO + O_2 \quad (1)$$

$$HSO + O_3 \rightarrow HS + 2O_2 \quad (2)$$

There have been numerous experimental and theoretical studies of the HSO and HOS isomers.[11−28] Ab initio calculations for the HSO and HOS radicals were first reported by Sannigrahi et al.,[26] who predicted HOS to be more stable than HSO. Several ab initio calculations[7] have been reported afterward which corroborated such a prediction, although the magnitude of the energy difference between the minima associated with these species was found to decrease with improvement in the quality of the calculations. In fact, it was pointed out by Xantheas and Dunning[27] that failure to account for dynamical correlation and the inadequacy of the basis sets were the main reasons why earlier calculations led to poor geometries and failed to correctly predict the relative stability of HSO and HOS. It seems well-established[7] now that HSO is more stable than HOS. However, most ab initio calculations so far reported have been devoted to studying the minima and the transition state for the isomerization process. An exception is the work by Xantheas and Dunning,[27] who have computed the minimum energy paths for the addition of H to SO to form HSO and HOS. In the present work, we report novel full valence complete active space (FVCAS) and multireference configuration interaction (MRCI) calculations covering over 500 geometries, including the minima, transition states, and S−H−O geometries. Moreover, we have subsequently corrected the calculated ab initio energies by means of the double many-body expansion-scaled external correlation (DMBE-SEC) method[29] to account for the complete basis set/complete CI limits. The resulting DMBE-SEC energies have then been used to calibrate a potential energy surface based on the DMBE[30−33] formalism (see also ref 34). This potential energy surface shows the correct long-range behavior at all dissociation channels and provides a realistic representation at all interatomic separations, especially those covered by the calculated ab initio energies.

The paper is organized as follows. Section 2 describes the ab initio calculations carried out in the present work. In section 3, we deal with the representation of the DMBE potential energy surface. Specifically, section 3.1 focuses on the two-body energy terms, while section 3.2 concentrates on the three-body energy terms. The main topographical features of the DMBE potential energy surface are discussed in section 4. Some concluding remarks are in section 5.

2. Ab Initio Calculations

The ab initio calculations have been carried out at the MRCI[35] level with a FVCAS[36,37] as the reference wave function. For the basis set, we have selected the aug-cc-pvtz (AVTZ) of Dunning,[38−40] with the calculations being carried out using the MOLPRO[41] package. A total of 500 grid points have been chosen to map the potential energy surface over the region defined by $2.61 \le r/a_0 \le 8.76$, $1.91 \le R/a_0 \le 6.73$, and $0 \le \gamma/\text{deg} \le 180$. The Jacobi coordinates r, $\mathbf{R}$, and γ are defined in Figure 1: r is the SO distance, $\mathbf{R}$ is the vector associated with the atom−diatom separation connecting the H atom to the geometrical center of SO, and γ is defined by $\cos\gamma = r\mathbf{R}/|r\mathbf{R}|$. We have also studied at the same level of theory the complicated potential energy curves for SO, SH, and OH (78 points in all). The ab initio energies determined in this way were subsequently corrected by using the DMBE-SEC method[32] to account for the excitations beyond singles and doubles and, more importantly, for the incompleteness of the one-electron basis set.

10.1021/jp0101460 CCC: $20.00
Published on Web 05/22/2001

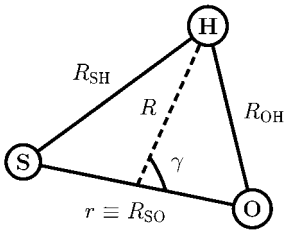

Figure 1. Coordinate system used in the present work.

In the DMBE-SEC method, the total interaction energy of the triatomic is written as[29]

$$V(\mathbf{R}) = V_{\mathrm{FVCAS}}(\mathbf{R}) + V_{\mathrm{DMBE-SEC}}(\mathbf{R}) \tag{3}$$

where

$$V_{\mathrm{FVCAS}}(\mathbf{R}) = \sum_{\mathrm{AB}} V^{(2)}_{\mathrm{AB,FVCAS}}(R_{\mathrm{AB}}) + V^{(3)}_{\mathrm{ABC,FVCAS}}(R_{\mathrm{AB}},R_{\mathrm{BC}},R_{\mathrm{AC}}) \tag{4}$$

$$V_{\mathrm{DMBE-SEC}}(\mathbf{R}) = \sum_{\mathrm{AB}} V^{(2)}_{\mathrm{AB,DMBE-SEC}}(R_{\mathrm{AB}}) + V^{(3)}_{\mathrm{ABC,DMBE-SEC}}(R_{\mathrm{AB}},R_{\mathrm{BC}}R_{\mathrm{AC}}) \tag{5}$$

and the summations extend to all diatomic fragments. In turn, the three-body energy term of the SEC series expansion assumes the form

$$V^{(2)}_{\mathrm{AB,DMBE-SEC}}(R_{\mathrm{AB}}) = [V^{(2)}_{\mathrm{AB,FVCAS-CISD}}(R_{\mathrm{AB}}) - V^{(2)}_{\mathrm{AB,FVCAS}}(R_{\mathrm{AB}})]/F^{(2)}_{\mathrm{AB}} \tag{6}$$

$$V^{(3)}_{\mathrm{ABC,DMBE-SEC}}(R_{\mathrm{AB}},R_{\mathrm{BC}},R_{\mathrm{AC}}) = [V^{(3)}_{\mathrm{ABC,FVCAS-CISD}}(R_{\mathrm{AB}},R_{\mathrm{BC}},R_{\mathrm{AC}}) - V^{(3)}_{\mathrm{ABC,FVCAS}}(R_{\mathrm{AB}},R_{\mathrm{BC}},R_{\mathrm{AC}})]/F^{(3)}_{\mathrm{ABC}} \tag{7}$$

where $F^{(2)}_{\mathrm{AB}}$ is a parameter being chosen to reproduce the bond dissociation energy of the corresponding AB diatomic. Because of the lack of similar spectroscopic information on the well-depth of the triatomic, the corresponding three-body factor $F^{(3)}_{\mathrm{ABC}}$ has been taken as the average of the two-body F-factors. Such a procedure, originally tested[29] on ground-state HO_2, led in the present case to the values $F^{(2)}_{\mathrm{SO}} = 0.6850$, $F^{(2)}_{\mathrm{SH}} = 0.7713$, $F^{(2)}_{\mathrm{OH}} = 0.7826$, and $F^{(3)}_{\mathrm{HSO}} = 0.7463$.

3. DMBE Potential Energy Surface for HSO

3.1. Two-Body Energy Terms. The diatomic potential energy curves have been modeled using the extended Hartree−Fock approximation correlation energy method for diatomics, including the united atom limit (EHFACE2U),[42] with the available parameters being determined by fitting experimental and ab initio data. They assume the general form[31,42]

$$V(R) = V_{\mathrm{EHF}} + V_{\mathrm{dc}} \tag{8}$$

where EHF refers to the extended Hartree−Fock type energy and dc is the dynamical correlation energy. As usual, the latter is modeled semiempirically by[43]

$$V_{\mathrm{dc}}(R) = -\sum_{n=6,8,10} \chi_n(R)\frac{C_n}{R^n} \tag{9}$$

with the damping functions for the dispersion coefficients

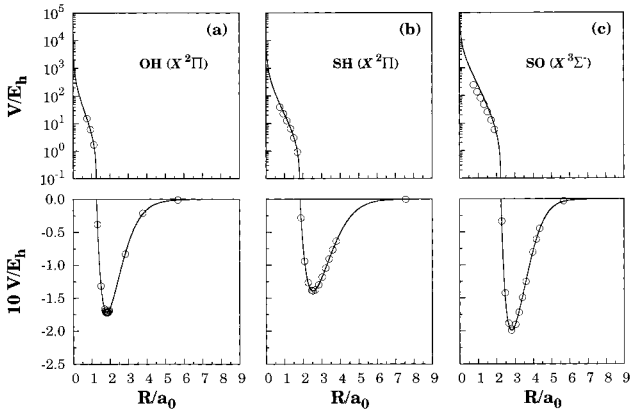

Figure 2. EHFACE2U potential energy curves: (a) OH($X^2\Pi$), (b) SH($X^2\Pi$), and (c) SO($X^3\Sigma^-$). The circles indicate the ab initio points and the lines the EHFACE2U values.

assuming the form

$$\chi_n(R) = \left[1 - \exp\left(-A_n\frac{R}{\rho} - B_n\frac{R^2}{\rho^2}\right)\right]^n \tag{10}$$

In eq 10, A_n and B_n are auxiliary functions defined by

$$A_n = \alpha_0 n^{-\alpha_1} \tag{11}$$

$$B_{\mathrm{n}} = \beta_0 \exp(-\beta_1 n) \tag{12}$$

where α_0, b_0, α_1, and β_1 are universal dimensionless parameters for all isotropic interactions[30,31] $\alpha_0 = 16.36606$, $\alpha_1 = 0.70172$, $b_0 = 17.19338$, and $\beta_1 = 0.09574$. Moreover, the scaling parameter ρ is defined as

$$\rho = 5.5 + 1.25R_0 \tag{13}$$

where $R_0 = 2(\langle r_{\mathrm{X}}^2\rangle^{1/2} + \langle r_{\mathrm{Y}}{}^2\rangle^{1/2})$ is the LeRoy[44] distance for onset of the undamped R^{-n} series expansion and $\langle r_{\mathrm{X}}^2\rangle$ is the expectation value of the squared radius for the outermost electrons of atom X (similarly for atom Y). Finally, the exponentially decaying part of the EHF-type energy term is represented by the general form

$$V_{\mathrm{EHF}}(R) = -\frac{D}{R}(1 + \sum_{i=1}^{3} a_i r^i)\exp(-\gamma r) \tag{14}$$

where

$$\gamma = \gamma_0[1 + \gamma_1 \tanh(\gamma_2 r)] \tag{15}$$

where $r = R - R_{\mathrm{e}}$ is the displacement coordinate from the equilibrium diatomic geometry; D, a_i ($i = 1 \rightarrow 3$), and γ_i ($i = 0 \rightarrow 2$) are adjustable parameters to be obtained as described elsewhere.[31,42]

For the ground-state hydroxyl radical OH($X^2\Pi$), we have used a potential energy curve previously reported by one of us and Voronin[45] which has been calibrated using Rydberg−Klein−Rees (RKR)-type data. Figure 2a shows that the potential energy function so obtained also reproduces our calculated ab initio energies.

For the sulfur hydride ground state, SH($X^2\Pi$), there is no RKR experimental data, and hence, we have used our own ab initio points and the experimental dissociation energy[46] in the

TABLE 1: Long-Range Coefficients for the Diatomic Fragments in au

	R_0	C_6	C_8	C_{10}
SO($X^3\Sigma^-$)	7.3119	53.09	1206.5	30982.5
SH($X^2\Pi$)	7.9652	34.49	896.5	26332.1
OH($X^2\Pi$)	6.2949	11.47	195.0	4342.3

TABLE 2: Parameters of the Two-Body Hartree−Fock Energy in au

	SO($X^3\Sigma^-$)	SH($X^2\Pi$)	OH($X^2\Pi$)
R_e	2.7988	2.5334	1.8344
D	0.479589	0.308372	0.275865
a_1	2.2594	1.8997	2.2904
a_2	1.2128	0.7234	1.0466
a_3	1.0265	0.2562	0.5147
γ_0	1.7823	1.4139	1.7110
γ_1	3.6305	6.3459	1.9222
γ_2	0.0458	0.0146	0.0747

TABLE 3: Numerical Values, in au, of the Parameters in Eq 19

S−OH	$C_6(R)$	$C_8(R)$	$C_{10}(R)$
R_M	4.0	4.0	4.0
D_M	34.28	1044.0	34824.0
a_1	−0.0150	−0.0751	−0.0987
a_2	−0.2371	−0.2452	−0.2481
a_3	0.0860	0.1014	0.1073
b_2	0.1532	0.1696	0.1799
b_3	0.0068	0.0122	0.0137
O−SH	$C_6(R)$	$C_8(R)$	$C_{10}(R)$
R_M	4.94	4.93	4.92
D_M	17.13	537.2	17643.0
a_1	−0.1269	−0.1603	−0.1842
a_2	−0.1776	−0.1712	−0.1677
a_3	0.0863	0.0879	0.0903
b_2	0.1741	0.1830	0.1919
b_3	0.0188	0.0203	0.0216
H−SO	$C_6(R)$	$C_8(R)$	$C_{10}(R)$
R_M	5.29	5.41	5.49
D_M	16.20	457.7	14495.0
a_1	0.7627	0.7699	0.7739
a_2	0.1331	0.1238	0.1177
a_3	0.0009	0.0006	0.0012
b_2	0.0784	0.1018	0.1219
b_3	1.0×10^{-6}	0.0009	0.0006

fitting procedure. Figure 2b shows that the model potential accurately reproduces the ab initio energies while showing good ability for extrapolation to the regions not covered by the fitted data. The sulfur oxide ground-state SO($X^3\Sigma^-$) potential energy curve has been calibrated by fitting our FVCAS-SEC energies and the experimental RKR points of Singh et al.[47] in conjunction with the recent heat of formation determined by Clerbaux et al.[48] Except for the last inner ab initio points, Figure 2c shows that the data is represented quite reliably. However, at very short distances, the ab initio points may not be as accurate, while the EHFACE2U model leads by construction to the proper united-atom limit of the collapsed diatomic ($R \rightarrow 0$). The numerical values of all diatomic parameters are gathered in Table 1 and Table 2.

3.2. Three-Body Energy Terms. Following the usual procedure[30−33] (see also ref 34), we split the three-body energy into several contributions. Specifically, one has the extended Hartree−Fock and dynamical correlation parts, with the electrostatic component of the EHF part also considered independently. In the following subsections, we provide a description of each component. To represent the three-body dynamical

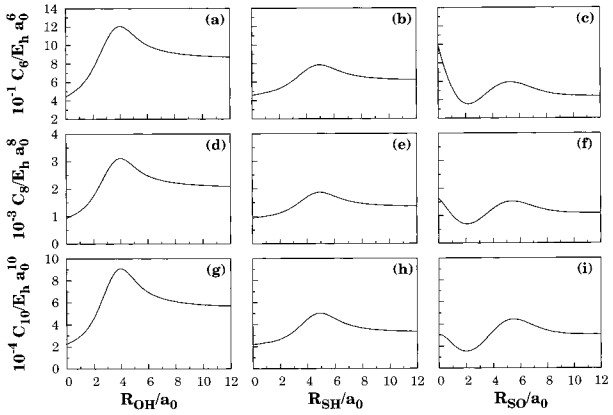

Figure 3. Dispersion coefficients for the atom−diatom asymptotic channels of HSO as a function of the corresponding intramolecular distance. The C_6 coefficients are displayed in panels a for S−OH, b for O−SH and c for H−SO. Panels d−f show the corresponding C_8 coefficients and g−i those of C_{10}.

correlation and the electrostatic energies, we have chosen the general form proposed by one of authors,[49] namely

$$V^{(3)}_{dc,ele} = \sum_i \sum_n f_i(\mathbf{R}) C_n^{(i)}(R_i,\theta_i)\chi_n(r_i) r_i^{-n} \qquad (16)$$

where i labels the I−JK channel associated with the center of mass separation r_i, R_i is the J−K bond distance, and $\cos\theta_i = \vec{r}_i\vec{R}_i/|\vec{r}_i\vec{R}_i|$; for the notation, see Figure 1 of ref 32. In turn, $C_n^{(i)}(R_i,\theta_i)$ are electrostatic coefficients when $n = 4$ or 5, representing the dipole−quadrupole and quadrupole−quadrupole interactions. For $n = 6$, 8, and 10, $C_n^{(i)}(R_i,\theta_i)$'s represent atom−diatom dispersion coefficients given by

$$C_n^{(i)} = \sum_L C_n^L P_L(\cos\theta_i) \qquad (17)$$

where $P_L(\cos\theta_i)$ denotes the L-th term of the Legendre polynomial expansion and C_n^L is the associated expansion coefficient. Additionally, the function $\chi_n(r_i)$ in eq 16 is the corresponding diatomic damping function given by eq 10. Moreover, $f_i(\mathbf{R})$ is a switching function chosen from the requirement that it must be +1 for $R_i = R_i^e$ and $r_i \rightarrow \infty$ and 0 for $R_i \rightarrow \infty$. Following previous work,[49] we have employed the form

$$f_i = \frac{1}{2}\{1 - \tanh[\xi(\eta s_i - s_j - s_k)]\} \qquad (18)$$

where $s_i = R_i - R_i^e$ (corresponding expressions apply for s_j, s_k, f_k, and f_k), and η is a constant chosen to ensure the proper asymptotic behavior; as before,[49] we have chosen the value $\eta = 3$ such as to satisfy the proper asymptotic limits. Furthermore, the parameter ξ has been taken as the average of the exponents of the OH and SH range decaying factors in the three-body term: $\xi = 0.58a_0^{-1}$. Regarding the damping functions $\chi_n(r_i)$, we still adopt eq 10 but replace R by the center-of-mass separation for the relevant atom−diatom channel. Additionally, the value of ρ has been assumed as the average value of the corresponding OH and SH diatomic scaling parameters. Finally, r_i has been approximated[31] by $r_i = (R_j + R_k)/2$.

3.2.1. Three-Body Dynamical Correlation Energy. Following previous work,[49] only the spherically averaged components ($L = 0$) of the atom−diatom dispersion coefficients have been considered, with the involved internuclear dependences being

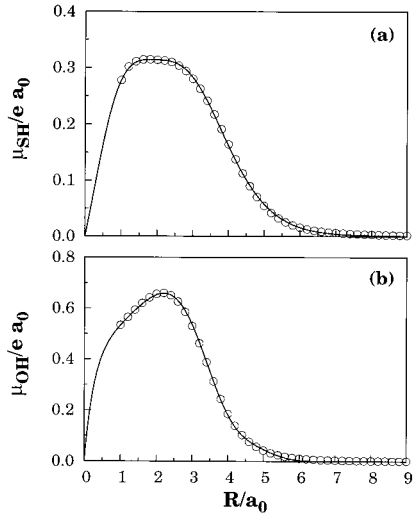

Figure 4. Variation of the OH (a) and SH (b) dipole moments with internuclear distance. Circles indicate MR−CISD points, while the lines indicate the results predicted from eq 22.

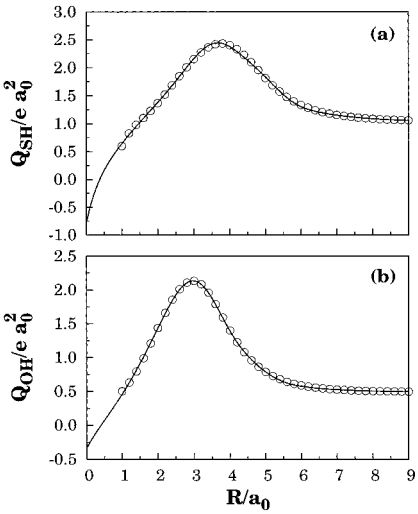

Figure 5. Variation of the OH (a) and SH (b) quadrupole moments with internuclear distance. Circles indicate the MR−CISD points, while the lines show the results predicted from eq 23.

estimated as reported elsewhere,[50] i.e., by using the dipolar isotropic polarizabilities (calculated in this work at the MRCI level of theory), combined with a generalized Slater−Kirkwood approximation.[51] The atom−diatom dispersion coefficients were then fitted to the form

$$C_n^{A-BC}(R) = C_n^{AB} + C_n^{AC} + D_M(1 + \sum_{i=1}^{3} a_i r^i)\exp(-\sum_{i=1}^{3} b_i r^i) \quad (19)$$

where $r = R - R_M$ is the displacement relative to the position of the maximum and $b_1 \equiv a_1$. The parameters that resulted from the fits are reported in Table 3, and the internuclear dependences of the dispersion coefficients are shown in Figure 3.

As pointed out elsewhere,[49] eq 16 causes an overestimation of the dynamical correlation energy at the atom−diatom dissociation channel. To correct such a behavior, we have multiplied the two-body dynamical correlation energy for the *i*-th pair by $f_i(\mathbf{R})$ and, correspondingly, for the channels *j* and *k*. This ensures[49] that the only two-body contribution at the *i*-th channel is that of JK.

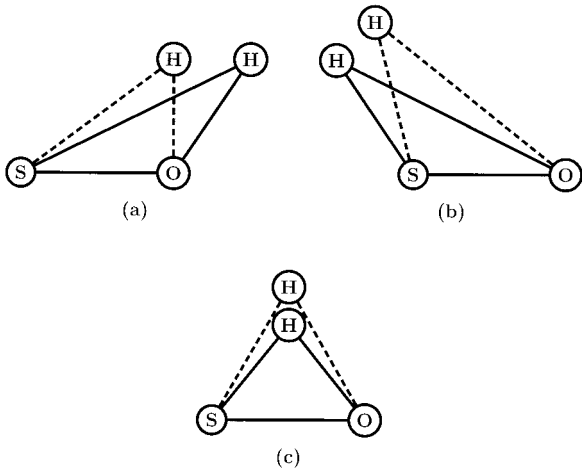

Figure 6. Reference geometries used in the present work for the three-body EHF part of the potential energy surface: (a) HOS, (b) HSO, and (c) transition state for reaction HSO → HOS. The solid lines represent the equilibrium geometries of the corresponding stationary points, while the dotted lines show the reference geometries which have been actually employed.

TABLE 4: Numerical Values, in au, for OH and SH Dipole Moments in Eq 22

	OH	SH
R_M	2.20	1.8
D_M	0.658585	0.314426
a_1	−0.29843	0.189345
a_2	−0.174482	−0.165016
a_3	0.0762564	0.0174276
b_2	0.0204867	0.0134371
b_3	0.1171210	0.000001

TABLE 5: Numerical Values, in au, for OH and SH Quadrupole Moments in Eq 23

	OH	SH
R_M	3.0	3.7
M_6	5500	21 000
D_M	1.127	0.65607488
a_1	−0.314458	0.01782770
a_2	−0.254650	−0.1186250
a_3	0.2301120	0.54471800
b_1	−0.373896	−0.0758723
b_2	0.5226040	0.70193800
b_3	0.1344000	0.14595400
Q_∞	0.49	1.05

3.2.2. Three-Body Electrostatic Energy. Since the H atom has spherical symmetry, we have to consider only the interactions of the oxygen and sulfur quadrupoles with the SH and OH dipole and quadrupolar moments. Thus, a total of four electrostatic interactions have been taken into account. As stated above, eq 16 has been employed to write the electrostatic energy, and in this case, $C_n(R_i,\theta_i)$'s are electrostatic coefficients. If the Buckingham convention is used,[52] such coefficients assume the form

$$C_{4,ele}(R_{AB},\theta) = \frac{3}{2}\mu_{AB}Q_C A_{DQ}(\theta_a,\theta_b,\phi_{ab}) \quad (20)$$

$$C_{5,ele}(R_{AB},\theta) = \frac{3}{4}Q_{AB}Q_C A_{QQ}(\theta_a,\theta_b,\phi_{ab}) \quad (21)$$

where the indexes AB and C stand for OH (SH) and S (or O), respectively. The functional forms of A_{DQ} and A_{QQ} were those employed in previous work[53] based on the so-called classical optimized quadrupole[54] model, according to which the

TABLE 6: Numerical Values of the Coefficients of Polynomial A in the Three-Body Extended Hartree−Fock Energy in au

$\gamma_1^A = 0.85$ $R_1^{A,\mathrm{ref}} = 3.30$	$\gamma_2^A = 0.58$ $R_2^{A,\mathrm{ref}} = 3.56$	$\gamma_3^A = 0.49$ $R_3^{A,\mathrm{ref}} = 1.73$
$c_{000}^A = -0.152971042$	$c_{001}^A = -0.0106451758$	$c_{002}^A = 0.02841603$
$c_{003}^A = 0.410335814$	$c_{004}^A = -0.0186074137$	$c_{005}^A = 0.0243697848$
$c_{010}^A = -0.0318850512$	$c_{011}^A = 0.0773253466$	$c_{012}^A = 0.352135922$
$c_{013}^A = 0.196064485$	$c_{014}^A = -0.0801457935$	$c_{020}^A = 0.328257694$
$c_{021}^A = -0.841754198$	$c_{022}^A = 0.241822527$	$c_{023}^A = 0.135119134$
$c_{030}^A = -0.23207117$	$c_{031}^A = -0.495856539$	$c_{032}^A = -0.101029651$
$c_{040}^A = 0.10834947$	$c_{041}^A = 0.0439618526$	$c_{050}^A = 0.0777769216$
$c_{100}^A = -0.160730172$	$c_{101}^A = -0.145518002$	$c_{102}^A = 0.708973954$
$c_{103}^A = 0.221896139$	$c_{104}^A = 0.0335980733$	$c_{110}^A = -0.368934267$
$c_{111}^A = -0.0399540713$	$c_{112}^A = 0.54277435$	$c_{113}^A = -0.0953548204$
$c_{120}^A = 0.250767376$	$c_{121}^A = -0.0443403774$	$c_{122}^A = 0.423678731$
$c_{130}^A = -0.200739683$	$c_{131}^A = -0.148990628$	$c_{140}^A = 0.00673609579$
$c_{200}^A = 0.231212503$	$c_{201}^A = -0.571911856$	$c_{202}^A = 0.615185605$
$c_{203}^A = -0.00488797525$	$c_{210}^A = -0.612887845$	$c_{211}^A = 0.44185333$
$c_{212}^A = -0.255883112$	$c_{220}^A = -0.0467274605$	$c_{221}^A = 0.62569975$
$c_{230}^A = 0.265091203$	$c_{300}^A = -0.947014418$	$c_{301}^A = 0.414265497$
$c_{302}^A = 0.0481590732$	$c_{310}^A = 0.441634224$	$c_{311}^A = -0.560754057$
$c_{320}^A = 0.279140359$	$c_{400}^A = 0.368292954$	$c_{401}^A = 0.0417331533$
$c_{410}^A = -0.0497157716$	$c_{500}^A = 0.0184014022$	

TABLE 7: Numerical Values of the Coefficients of Polynomial B in the Three-Body Extended Hartree−Fock Energy in au

$\gamma_1^B = 0.92$ $R_1^{B,\mathrm{ref}} = 2.80$	$\gamma_2^B = 0.58$ $R_2^{B,\mathrm{ref}} = 2.68$	$\gamma_3^B = 0.53$ $R_3^{B,\mathrm{ref}} = 4.25$
$c_{000}^B = 0.34268533$	$c_{001}^B = -0.156266035$	$c_{002}^B = -0.294456751$
$c_{003}^B = -0.104628235$	$c_{004}^B = -0.0395350302$	$c_{005}^B = -0.0258194682$
$c_{010}^B = -0.283879354$	$c_{011}^B = 0.0249695419$	$c_{012}^B = -0.399127497$
$c_{013}^B = 0.160709558$	$c_{014}^B = -0.0491731653$	$c_{020}^B = -0.873890432$
$c_{021}^B = 0.00383147459$	$c_{022}^B = -0.152090755$	$c_{023}^B = -0.0320679312$
$c_{030}^B = 0.755325919$	$c_{031}^B = 0.408332247$	$c_{032}^B = 0.0708306864$
$c_{040}^B = 0.127078787$	$c_{041}^B = -0.0975231701$	$c_{050}^B = -0.114607354$
$c_{100}^B = -0.289964039$	$c_{101}^B = -0.230472236$	$c_{102}^B = 0.0972749497$
$c_{103}^B = -0.110590724$	$c_{104}^B = -0.0994307523$	$c_{110}^B = -0.550630406$
$c_{111}^B = -0.243992429$	$c_{112}^B = 0.0311063194$	$c_{113}^B = -0.198198673$
$c_{120}^B = 0.555584386$	$c_{121}^B = -0.370295745$	$c_{122}^B = 0.0569126419$
$c_{130}^B = 0.360760901$	$c_{131}^B = 0.170133025$	$c_{140}^B = -0.157920036$
$c_{200}^B = -0.756021158$	$c_{201}^B = -0.0522933035$	$c_{202}^B = -0.0476056622$
$c_{203}^B = -0.097395365$	$c_{210}^B = 0.645931587$	$c_{211}^B = 0.280831417$
$c_{212}^B = -0.20040811$	$c_{220}^B = 0.353531971$	$c_{221}^B = 0.0319832695$
$c_{230}^B = -0.0734865405$	$c_{300}^B = -0.60602039$	$c_{301}^B = 0.020614987$
$c_{302}^B = 0.0251193461$	$c_{310}^B = -0.051336385$	$c_{311}^B = 0.119990554$
$c_{320}^B = 0.0147474065$	$c_{400}^B = -0.0116238618$	$c_{401}^B = 0.205238381$
$c_{410}^B = 0.0734593641$	$c_{500}^B = 0.0775702596$	

atomic quadrupole adiabatically adjusts its angular orientation to that of the diatomic molecule to give the lowest interaction energy.

The analytical expression for the OH and SH dipoles have been obtained by fitting our own ab initio results to the form[55]

$$\mu(R) = D_{\mathrm{M}}(1 + \sum_{i=1}^{3} a_i r^i) \exp(-\sum_{i=1}^{3} b_i r^i) \qquad (22)$$

where $r = R - R_{\mathrm{M}}$ is the displacement relative to the maximum in $\mu(R)$ and $b_1 \equiv a_1$. In turn, the analytical expression for the intramolecular dependence of the quadrupoles has been chosen to be that previously employed by one of the authors and Rodrigues[56]

$$Q(R) = D_{\mathrm{M}}(1 + \sum_{i=1}^{3} a_i r^i) \exp(-\sum_{i=1}^{3} b_i r^i) + Q_\infty + \chi_8(R)\frac{M_6}{R^6} \qquad (23)$$

where $r = R - R_{\mathrm{M}}$ now in the displacement relative to the maximum in $Q(r)$. The input data for the permanent electric moments has been obtained from ab initio MRCI calculations carried out in the present work. The numerical values of the parameters for the dipole and quadrupole moments using the above equations are given in Tables 4 and 5, while the graphical representation of the dipole and quadrupole as a function of the diatomic bond distance is depicted in Figures 4 and 5.

3.2.3. Three-Body Extended Hartree−Fock Energy. By subtracting, for a given triatomic geometry, the sum of the two-body energy terms from the corresponding DMBE-SEC interaction energies (defined with respect to the infinitely separated ground-state atoms), one obtains the total three-body energy. Then, by subtracting the three-body electrostatic and dynamical correlation contributions from the total three-body energy calculated above, one gets the remaining three-body extended Hartree−Fock energy contribution. This is represented by using the form

TABLE 8: Numerical Values of the Coefficients of Polynomial C in the Three-Body Extended Hartree−Fock Energy in au

$\gamma_1^C = 0.76$ $R_1^{C,\mathrm{ref}} = 3.35$	$\gamma_2^C = 0.61$ $R_2^{C,\mathrm{ref}} = 3.00$	$\gamma_3^C = 0.50$ $R_3^{C,\mathrm{ref}} = 3.04$
$c^C_{000} = -0.0368229496$	$c^C_{001} = -0.129003395$	$c^C_{002} = 0.20818244$
$c^C_{003} = -0.215560967$	$c^C_{004} = 0.0327436241$	$c^C_{005} = -0.00277579984$
$c^C_{010} = -0.344210958$	$c^C_{011} = 0.31920124$	$c^C_{012} = 0.676245148$
$c^C_{013} = -0.0588732027$	$c^C_{014} = 0.0626825399$	$c^C_{020} = -1.01984483$
$c^C_{021} = -1.06002701$	$c^C_{022} = -0.285430471$	$c^C_{023} = -0.0121593163$
$c^C_{030} = 0.0989442215$	$c^C_{031} = 0.0487608753$	$c^C_{032} = -0.0346353473$
$c^C_{040} = 0.442210508$	$c^C_{041} = 0.0155389963$	$c^C_{050} = 0.0192298535$
$c^C_{100} = -0.178793571$	$c^C_{101} = -0.647450641$	$c^C_{102} = -0.545972629$
$c^C_{103} = 0.0671127689$	$c^C_{104} = 0.0147832243$	$c^C_{110} = -0.192412049$
$c^C_{111} = 0.511735943$	$c^C_{112} = -0.0906728726$	$c^C_{113} = -0.0121194958$
$c^C_{120} = -0.283103789$	$c^C_{121} = -0.0710891685$	$c^C_{122} = -0.0971627429$
$c^C_{130} = 0.167061534$	$c^C_{131} = -0.135636288$	$c^C_{140} = -0.150887754$
$c^C_{200} = -0.0535259653$	$c^C_{201} = -0.699043015$	$c^C_{202} = -0.0428548027$
$c^C_{203} = 0.0128170641$	$c^C_{210} = -0.680231297$	$c^C_{211} = 0.188599247$
$c^C_{212} = -0.0217923261$	$c^C_{220} = 0.507919222$	$c^C_{221} = -0.0884283396$
$c^C_{230} = -0.0990154673$	$c^C_{300} = 0.392368471$	$c^C_{301} = -0.614484326$
$c^C_{302} = 0.0507822473$	$c^C_{310} = 0.5668414$	$c^C_{311} = 0.121341497$
$c^C_{320} = -0.117210525$	$c^C_{400} = -0.445262241$	$c^C_{401} = 0.0612374732$
$c^C_{410} = -0.107519532$	$c^C_{500} = 0.0639223458$	

$$V_{\mathrm{EHF}}^{(3)} = \sum_{\mathrm{K}=A,B,C} \Big(\sum_{i=0}^{N_{\mathrm{K}}}{}' \sum_{j=0}^{N_{\mathrm{K}}}{}' \sum_{k=0}^{N_{\mathrm{K}}}{}' c_{ijk}^{\mathrm{K}} Q_1^i Q_2^j Q_3^k\Big) \prod_{i=1}^{3} \{1 - \tanh[\gamma_i^{\mathrm{K}}(R_i - R_i^{\mathrm{K,ref}})]\} \quad (24)$$

where $N_A = N_B = N_C = 5$, the prime means that the sum is restricted to $i + j + k \le 5$, and the symmetry coordinates are defined as

$$\begin{pmatrix} Q_1 \\ Q_2 \\ Q_3 \end{pmatrix} = \begin{pmatrix} \sqrt{\frac{1}{3}} & \sqrt{\frac{1}{3}} & \sqrt{\frac{1}{3}} \\ 0 & \sqrt{\frac{1}{2}} & -\sqrt{\frac{1}{2}} \\ \sqrt{\frac{2}{6}} & -\sqrt{\frac{1}{6}} & -\sqrt{\frac{1}{6}} \end{pmatrix} \begin{pmatrix} R_1 - R_1^{\mathrm{K,ref}} \\ R_2 - R_2^{\mathrm{K,ref}} \\ R_3 - R_3^{\mathrm{K,ref}} \end{pmatrix} \quad (25)$$

The complete set of parameters (186 in all) is 56 c_{ijk}, 3 γ_i, and 3 R_i^{ref}, for each polynomial (A, B, or C) in eq 24, having been obtained from a fit of the complete potential energy surface to our DMBE-SEC energies. Three polynomials of the same type and size (A, B, or C in eq 24) have been employed, one at each of the following stationary points: HSO, HOS, and HSO → HOS isomerization transition state (in that order). Thus, the origin of the displacement coordinates is for each polynomial taken to be close to the geometry of the corresponding stationary point. Figure 6 shows the reference geometries (broken lines) employed for the three polynomials in comparison with the geometries of HSO, HOS, and isomerization saddle point predicted by the DMBE potential energy surface (solid line). To obtain $R_i^{\mathrm{K,ref}}$, we have first assumed their values to be the equilibrium geometries and, subsequently, optimized them through a trial-and-error procedure by carrying out linear least-squares fits. The γ_i values have also been optimized in a similar way. The points included in the fits have been chosen with the condition that the total energy does not exceed 300 kcal mol^{-1} with respect to the HSO minimum. This procedure reduced the number of fitted points to 461. The numerical values of the parameters obtained from such a procedure are listed in Tables 6−8.

Table 9 shows the stratified root-mean-squared deviations (rmsd) of the final fit with respect to the fitted and nonfitted ab initio energies. As seen from Table 9, the final potential energy surface is able to fit 461 points (with energies up to 300 kcal mol^{-1}) with an accuracy of ca. 1 kcal mol^{-1}. Also seen from Table 9 is the fact that the nonfitted points are well reproduced by the DMBE potential energy surface of the present work; the rmsd is 2.8 kcal mol^{-1} for all points below 500 kcal mol^{-1}.

TABLE 9: Stratified Root-mean-square Deviations (in kcal mol^{-1}) of the DMBE Potential Energy Surface

E/(kcal mol^{-1})	N	rms[a]
5	20	0.654
10	53	0.723
20	66	0.692
30	73	0.790
40	85	0.822
50	107	0.866
60	129	0.853
70	198	0.841
80	230	0.849
90	261	0.910
100	309	0.987
110	348	0.997
120	369	1.040
130	397	1.051
140	404	1.053
150	410	1.064
160	418	1.060
170	430	1.058
180	443	1.075
200	453	1.076
300	461	1.069
400	466	*1.553*
500	477	*2.793*

[a] The values in italic imply that the points above the energy quoted in the first column have not been included in the fit.

4. Features of the Potential Energy Surface

The DMBE potential energy surface predicts the most stable minimum to be that associated with the HSO conformer. In fact, as seen from Table 10, HSO is 0.9 kcal mol^{-1} lower in energy than HOS. This result conforms with the most accurate theoretical predictions of Goumri et al.,[7] who have predicted from their G-2 calculations an energy difference of 2.1 kcal

TABLE 10: Stationary Points of the DMBE Potential Energy Surface[a]

	R_{OH}/a_0	R_{SH}/a_0	R_{SO}/a_0	E/kcal mol^{-1}	ω_1	ω_2	ω_3
HSO	4.4857	2.6190	2.8569	0.0[b]	998	1054	2181
	(4.3697)[c]	(2.6248)[c]	(2.8233)[c]		(1026)[c]	(1164)[c]	(2271)[c]
	(4.2502)[d]	(2.5511)[d]	(2.9102)[d]		(1013)[d]	(1063)[d]	(2570)[d]
HOS	1.8233	4.0819	3.0983	0.9[b]	839	1080	3783
				2.1[e]			
S···HO	1.8360	5.2513	7.0873	−3.3[f]	118	215	3739
SH···O	5.4670	2.5142	7.9812	−1.4[g]	80	104	2802
TS1	2.5679	2.7084	3.1668	46.7[b]	1711i	744	2354
				47.6[e]			
TS2	4.0509	6.0086	2.8296	1.7[h]	392i	291	1047
				1.8[i]			
TS3	7.1363	2.5335	6.3778	1.1[j]	97i	151	2725
TS4	1.8379	5.4132	6.5254	3.3[k]	139i	231	3758

[a] Harmonic frequencies are in cm^{-1}, and the experimental values are in parentheses when available. [b] Relative to the absolute minimum of HSO, −0.29615726E_h. [c] Experimental values from ref 16. [d] Experimental values from ref 11. [e] Best theoretical estimate, ref 7. [f] Relative to the energy of S + OH channel, −0.17020E_h. [g] Relative to the energy of O + SH channel, −0.13921E_h. [h] Relative to the energy of H + SO channel, −0.19901E_h. [i] Best theoretical estimate, ref. 27. [j] Relative to the minimum SH···O. [k] Relative to the minimum S···HO.

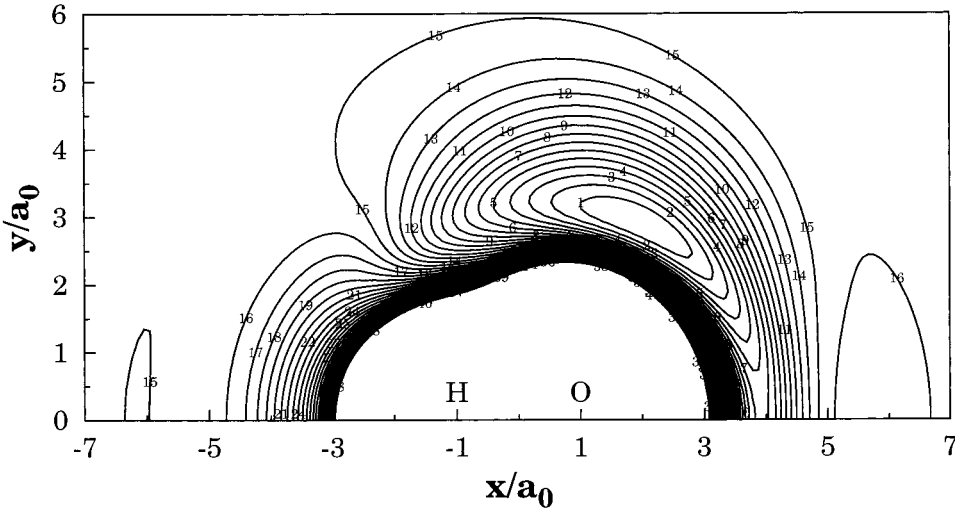

Figure 7. Contour plot for a S atom moving around the equilibrium OH molecule. Contours start at −0.287E_h, with successive contours at intervals of −0.008E_h.

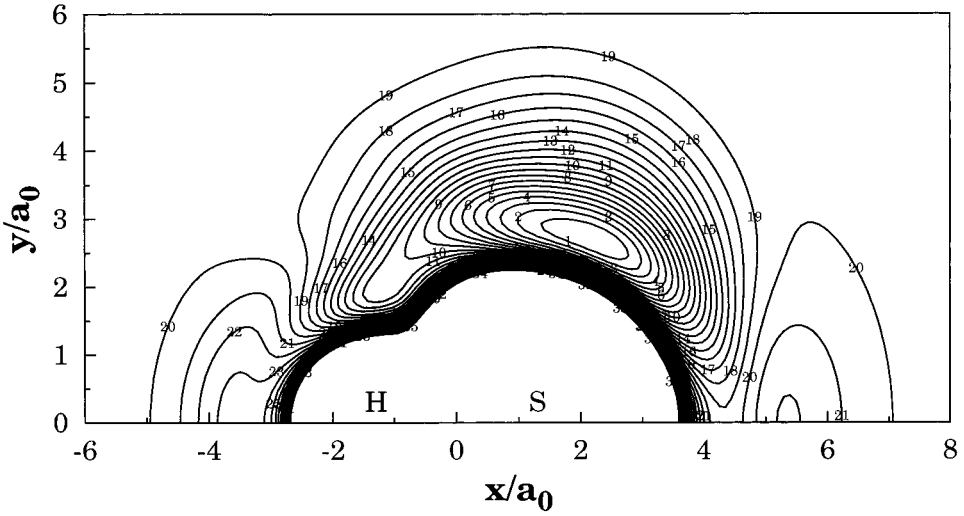

Figure 8. Contour plot for a O atom moving around the equilibrium SH molecule. Contours start at −0.287E_h, with successive contours at intervals of −0.008E_h.

mol^{-1}. We have also found two van der Waals minima, namely S···HO and SH···O, which lie 3.3 and 1.4 kcal mol^{-1} below the corresponding dissociation channels (S + OH or SH + O), respectively.

In Table 10, we report also four saddle points of index one. The first, labeled TS1, connects the two isomers HSO and HOS and is located 46.7 kcal mol^{-1} above the global minimum. Such an estimate agrees within 0.9 kcal mol^{-1} with the ab initio results

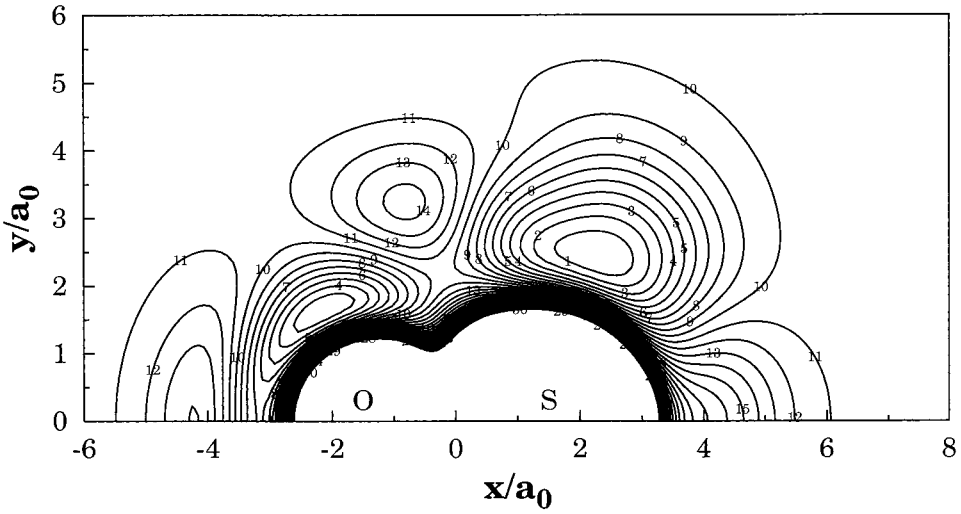

Figure 9. Contour plot for a H atom moving around the equilibrium SO molecule. Contours start at $-0.287E_h$, with successive contours at intervals of $-0.009E_h$.

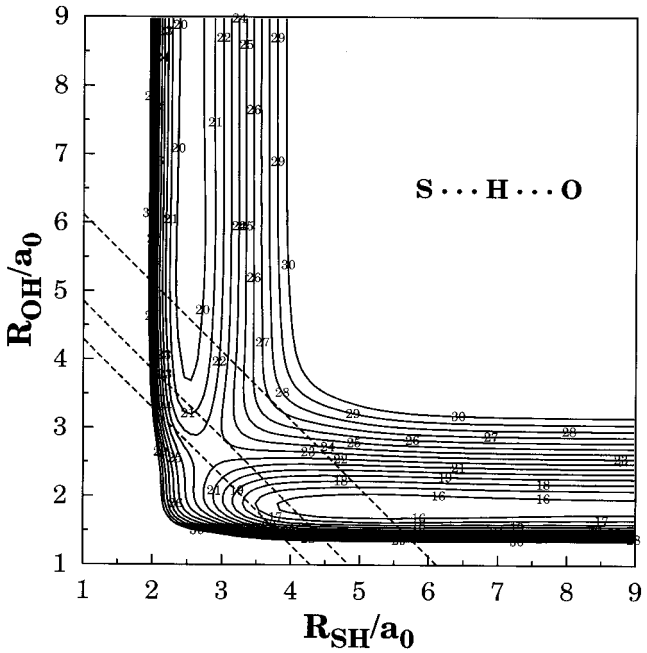

Figure 10. Stretching contour plot for linear S−H−O. Contours start at $-0.287E_h$, with successive contours at intervals of $-0.008E_h$. The dashed straight lines indicate the cuts associated with the curves shown in Figure 11.

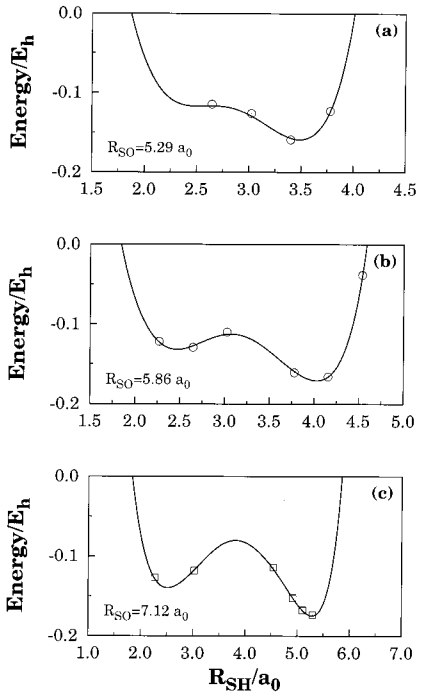

Figure 11. Potential energy curves for S−H−O linear configurations at fixed SO distances of (a) 5.29, (b) 5.86, and (c) 7.12 a_0. Also shown for comparison are the DMBE-SEC points of the present work: (○) points included in the fit; (△) points not included in the fit. See also Figure 10.

of Goumri et al.[7] and 0.1 kcal mol^{-1} with those of Xantheas and Dunning.[27] These authors suggested that such a large barrier might explain why only the isomer HSO is observed experimentally. The experimental geometry and frequencies of HSO are also included in Table 10 for comparison. The saddle point TS2 corresponds to a small barrier for the dissociation process HSO → H + SO and is located 1.5 kcal mol^{-1} above the dissociation limit; a value very similar to this one has also been obtained by Xantheas and Dunning[27] in their ab initio calculations (1.8 kcal mol^{-1}). In addition, the saddle points TS3 and TS4 have been found to connect the HSO or HOS isomers with the two van der Waals minima. Such stationary points lie 1.1 and 3.3 kcal mol^{-1} above the corresponding van der Waals minima.

Figure 7 shows a contour plot for a S atom moving around an equilibrium OH molecule. The main feature in this Figure is the HOS minimum. Also visible is a saddle point of index two which occurs for linear geometries.

In Figure 8, we show a contour plot for an O atom moving around an equilibrium SH molecule. The notable features in this plot are the HSO minimum and a saddle point of index two for linear geometries. In addition, there is a stationary point at high energies which appears as a minimum in the two-dimensional (2D) space scanned in the plot. Indeed, it corresponds in 3D to the isomerization transition state for the reaction HSO → HOS.

The plot for a H atom moving around an equilibrium SO molecule is shown in Figure 9. In this case, the minima associated with both isomers become clearly visible, as well as the isomerization transition state (TS1) connecting them. Not visible in the plot though is the transition state (TS2) for the H−atom dissociation process HOS → H + OS. Another important feature from this plot arises as a saddle point of index

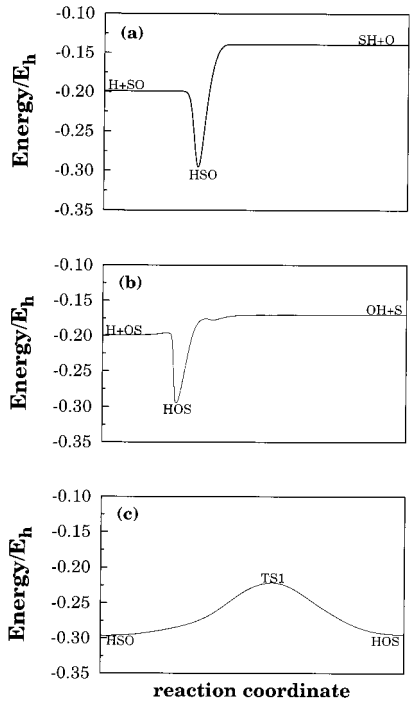

Figure 12. Minimum energy path for the reactions involving the (a) HSO isomer, (b) HOS, and (c) both.

two at the center of the plot. Looking like a maximum (apparently due to an avoided crossing), such a feature should trully be a cusp originated from the crossing of the two lowest electronic states.

Figure 10 shows a contour plot for linear S−H−O stretching. The main feature from this plot is the OH···S van der Waals minimum and a saddle point of index two connecting this minimum with the SH···O one, also visible in the figure. Also indicated by the dashed lines in this contour plot are cuts corresponding to the curves shown in Figure 11. These are depicted mainly to show that the agreement with the ab initio data is good, and hence, our predicted attributes for the OH···S hydrogen-bonded minimum should be reliable. In fact, as a test of our DMBE potential energy surface, and in order to verify the reliability of the hydrogen bonded structure OH···S, we have calculated additional (nonfitted) ab initio points at a fixed SO distance of $7.12a_0$. These points are displayed graphically in Figure 11c as a function of the SH distance with special symbols. Also shown in this Figure is the prediction of our DMBE potential surface. Clearly, the agreement between our fitted surface and the calculated points is quite satisfactory, suggesting that the OH···S hydrogen-bond structure is reliably described.

Figure 12 shows the minimum energy paths for the reactions H + SO → HS + O and H +SO → HO + S. Specifically, Figure 12a shows the minimum-energy path for the reaction H + SO → SH + O, which involves the global HSO minimum. As seen from this figure, there is no barrier for the dissociation process HSO → H + SO. In addition, the HSO → SH + O channel shows no barrier to dissociation either.

The minimum energy path for the process H + OS→ OH + S is shown in Figure 12b. Clearly, the relevant isomer is now HOS. Note that the HOS → H + OS dissociation process has a barrier (TS2), which is about 1.7 kcal mol^{-1} above the H + OS channel. In turn, the channel leading to OH + S has no barrier.

We have also computed the minimum energy path for the isomerization process HSO → HOS, which is shown in Figure 12c. Clearly, the two isomers (HSO and HOS) are connected by a saddle point of index 1 (TS1) located 46.6 kcal mol^{-1} above the HSO minimum.

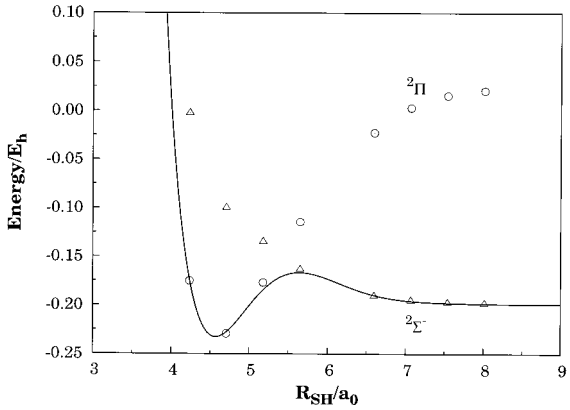

Figure 13. DMBE-SEC points for the $^2\Sigma^-$ (△) and $^2\Pi$ (○) states as a function of the HS bond distance. Also shown is the prediction of our DMBE potential energy surface.

Finally, we comment on the fact that our ab initio calculations predict a $^2\Sigma^-/^2\Pi$ crossing along the path for H approaching collinearly OS. Such a crossing is dictated by symmetry arguments, and hence becomes an avoided crossing at less symmetrical geometries (C_s). This is illustrated in Figure 13, which shows our DMBE-SEC points for the $^2\Sigma^-$ and $^2\Pi$ states as a function of the HS bond distance. Also shown in this figure is the prediction of our fitted DMBE single-valued potential energy surface. We observe that the fit is good but displays by built-in construction a smoothed maximum at regions where the crossing should take place.

5. Conclusions

We have reported a global single-valued DMBE form for the ground electronic state of HSO. This function has been calibrated from novel MR CISD ab initio energies after being corrected for the complete one-electron basis set/complete CI limit. This has been done using the DMBE-SEC method described elsewhere.[29] To improve the accuracy of the fit, we have introduced an *n*-body distributed polynomial approach, which implies using an individual multinomial development at the various stationary points. For simplicity, these have been restricted to the three most relevant ones corresponding to two minima (HSO, HOS) and the saddle point connecting them.

Acknowledgment. This work has been supported by the Fundação para a Ciência e Tecnologia, Portugal, under program PRAXIS XXI.

References and Notes

(1) Cuppit, L. T.; Gless, G. P. *Trans. Faraday Soc.* **1970**, *66*, 3007.
(2) Hollinden, G. A.; Kurylo, M. J.; Timmons, R. B. *J. Phys. Chem.* **1970**, *74*, 988.
(3) Takahashi, S. *Mem. Nat. Def. Acad. Jpn.* **1970**, *10*, 369.
(4) Whytock, D. A.; Timmons, R. B.; Lee, J. H.; Michael, J. V. *J. Chem. Phys.* **1976**, *65*, 2052.
(5) Slagle, I. R.; Baiochi, F.; Gutman, D. *J. Phys. Chem.* **1978**, *82*, 1333.
(6) Singleton, D. L.; Irwin, R. S.; Nip, W. S.; Cvetanovic, R. J. *J. Phys. Chem.* **1979**, *83*, 2195.
(7) Goumri, A.; Laakso, D.; Rocha, J.-D. R.; Smith, C. E.; Marshall, P. *J. Chem. Phys.* **1995**, *102*, 161.
(8) Black, G. J. *J. Chem. Phys.* **1984**, *80*, 1103.
(9) Friedl, R. R.; Brune, W. H.; Anderson, J. G. *J. Phys. Chem.* **1985**, *89*, 5505.
(10) Tyndall, G. S.; Ravishankara, A. R. *Int. J. Chem. Kinet.* **1991**, *23*, 483.

(11) Schurath, U.; Weber, M.; Becker, K. H. *J. Chem. Phys.* **1977**, *67*, 110.
(12) Benson, S. W. *Chem. Rev.* **1978**, *78*, 23.
(13) Hinchliffe, A. *J. Mol. Struct.* **1980**, *66*, 235.
(14) De, B. R.; Sannigrahi, A. B. *J. Comput. Chem.* **1980**, *1*, 334.
(15) Kamimoto, M.; Saito, S.; Hirota, E. *J. Mol. Spectrosc.* **1980**, *84*, 334.
(16) Ohashi, N.; Kamimoto, M.; Saito, S.; Hirota, E. *J. Mol. Spectrosc*. **1980**, *84*, 204.
(17) Sears, T. J.; McKellar, A. R. W. *Mol. Phys.* **1983**, *49*, 25.
(18) Luke, B. T.; McLean, A. D. *J. Phys. Chem.* **1985**, *89*, 4592.
(19) Plummer, P. L. *J. Chem. Phys.* **1990**, *92*, 6627.
(20) O'Hair, R. A. J.; DePuy, C. H.; Bierbaum, V. M. *J. Phys. Chem.* **1993**, *97*, 7955.
(21) Chang, Y.-T.; Loew, G. H. *Chem. Phys. Lett.* **1993**, *205*, 543.
(22) Espinosa-Garcia, J.; Corchado, J. C. *Chem. Phys. Lett*. **1994**, *218*, 128.
(23) Iraqui, M.; Golberg, N.; Schwarz, H. *J. Phys. Chem.* **1994**, *98*, 2015.
(24) Morris, V. R.; Jackson, W. M. *Chem. Phys. Lett.* **1994**, *223*, 445.
(25) Essefar, M.; Mó, O.; Yañez, M. *J. Chem. Phys.* **1994**, *101*, 2175.
(26) Sannigrahi, A. B.; Thunemmann, K. H.; Peyerimhoff, S. D.; Buenker, R. *J. Chem. Phys.* **1977**, *20*, 25.
(27) Xantheas, S. S.; Dunning, T. H., Jr. *J. Phys. Chem.* **1993**, *97*, 6616.
(28) Denis, P. A.; Ventura, O. N. *Int. J. Quantum Chem.* **2000**, *80*, 439.
(29) Varandas, A. J. C. *J. Chem. Phys.* **1989**, *90*, 4379.
(30) Varandas, A. J. C. *THEOCHEM* **1985**, *120*, 401.
(31) Varandas, A. J. C. *Adv. Chem. Phys.* **1988**, *74*, 255.
(32) Varandas, A. J. C. *Chem. Phys. Lett.* **1992**, *194*, 333.
(33) Varandas, A. J. C. In *Dynamical Processes in Molecular Physics*; Delgado-Barrio, G., Ed.; IOP Publishing: Bristol, U.K., 1993; p 3.
(34) Varandas, A. J. C In *Reaction and Molecular Dynamics*; Lagana, A., Riganelli, A., Eds.; Springer, Berlin, 2000l Vol. 75 of *Lecture Notes in Chemistry*, p 33.
(35) Werner, H.-J.; Knowles, P. J. *J. Chem. Phys.* **1988**, *89*, 5803.
(36) Werner, H.-J.; Knowles, P. J. *J. Chem. Phys.* **1985**, *82*, 5053.
(37) Knowles, P. J.; Werner, H.-J. *Chem. Phys. Lett.* **1985**, *115*, 259.
(38) Dunning, T. H., Jr. *J. Chem. Phys.* **1989**, *90*, 1007.
(39) Kendall, R.; Dunning, T. H., Jr.; Harrison, R. *J. Chem. Phys*. **1992**, *96*, 6769.
(40) Woon, D.; Dunning, T. H., Jr. *J. Chem. Phys*. **1993**, *98*, 1358.
(41) Werner, H.-J.; Knowles, P. J. MOLPRO is a package of ab initio programs written by H.-J. Werner and P. J. Knowles, with contributions from J. Almlöf, R D. Amos, M. J. O. Deegan, S. T. Elbert, C. Hampel, W. Meyer, K. A. Peterson, R. Pitzer, A. J. Stone, P. R Taylor, and R. Lindh, 1998.
(42) Varandas, A. J. C.; Silva, J. D. *J. Chem. Soc., Faraday Trans.* **1992**, *88*, 941.
(43) Varandas, A. J. C. *Mol. Phys.* **1987**, *60*, 527.
(44) Roy, R. J. L. *Spec. Period. Rep. Chem. Soc. Mol. Spectrosc*. **1973**, *1*, 113.
(45) Varandas, A. J. C.; Voronin, A. I. *Chem. Phys.* **1995**, *194*, 91.
(46) Wilson, S. H. S.; Hove, J. D.; Ashfold, M. N. R. *Mol. Phys.* **1996**, *88*, 841.
(47) Singh, A. N.; Rai, D. K. *J. Chem. Phys.* **1965**, *43*, 2151.
(48) Clerbaux, G.; Colin, R. *J. Mol. Struct.* **1994**, *165*, 334.
(49) Varandas, A. J. C. *J. Chem. Phys.* **1996**, *105*, 3524.
(50) Varandas, A. J. C.; Rodrigues, S. P. *J. Chem. Phys. Lett.* **1995**, *245*, 66.
(51) Matias, M. A.; Varandas, A. J. C. *Mol. Phys.* **1990**, *70*, 623.
(52) Buckingham, A. D. *Adv. Chem. Phys.* **1967**, *12*, 107.
(53) Varandas, A. J. C.; Rodrigues, S. P. J. *J. Chem. Phys.* **1997**, *106*, 9647.
(54) Varandas, A. J. C. *THEOCHEM* **1988**, *166*, 59.
(55) Varandas, A. J. C. In *Conferencias Plenarias de la XXIII Reunión Bienal de Química*; Feliciano, A. S., Grande, M., Casado, J., Eds.; Universidad de Salamanca: Salamanca, Spain, 1991; p 321.
(56) Rodrigues, S. P. J.; Varandas, A. J. C. *Phys. Chem. Chem. Phys*. **2000**, *2*, 435.